



Research article

Sanchi-mediated inactivation of IL1B accelerates wound healing through the NFκB pathway deficit

Xiaoling Li^{a,1}, Zhiwei Zhao^{b,*}, Bo Cui^b, Yanfeng Li^b^a Health Control Department, Luoyang Orthopedic Hospital of Henan Province (Orthopedic Hospital of Henan Province), Zhengzhou, 450016, Henan, PR China^b Department of Hand Surgery & Micro Orthopedics, Luoyang Orthopedic Hospital of Henan Province (Orthopedic Hospital of Henan Province), Zhengzhou, 450016, Henan, PR China

ARTICLE INFO

Keywords:

Keratinocytes
Microvascular endothelial cells
Traditional Chinese medicine
Hydrogels

ABSTRACT

Context: Sanchi promotes wound healing by repressing fibroblast proliferation.**Objective:** This study examined the effect of Sanchi on keratinocytes (KCs) and microvascular endothelial cells (MECs) and rats with skin injury.**Materials & methods:** Hydrogels containing different concentrations of Sanchi extract were prepared to observe wound closure over 10 days. SD rats were divided into the control, Hydrogel, 5% Hydrogel, 10% Hydrogel, 10% Hydrogel + Ad5-NC, and 10% Hydrogel + Ad5-IL1B groups. KCs and MECs were induced with H₂O₂ for 24 h. Cell viability, apoptosis, and the levels of inflammation- and oxidative stress-related factors were examined. The effect of IL1B on wound healing was also evaluated.**Results:** Compared to the Control group (83% ± 7.4%) or Hydrogel without Sanchi extract (84% ± 8.5%), Hydrogel with 5% (95% closure ± 4.0%) or 10% Sanchi extract (98% ± 1.7%) accelerated wound healing in rats and attenuated inflammation and oxidative stress. Hydrogels containing Sanchi extract increased collagen deposition and CD31 expression in tissues. H₂O₂ (100 μM) induced injury in KCs and MECs, whereas Sanchi rescued the viability of KCs and MECs. Sanchi inhibited cell inflammation and oxidative stress and decreased apoptosis. As Sanchi blocked the NFκB pathway via IL1B, IL1B mitigated the therapeutic effect of Sanchi.**Discussion and conclusion:** Sanchi demonstrated therapeutic effects on wound healing in rats by promoting KCs and MECs activity. These findings provide valuable information for the clinical application of Sanchi, which needs to be validated in future clinical trials.

1. Introduction

Wounds occur on many occasions during one's lifetime, and healing is a complex event that involves various key cellular and molecular contributors because many wounds create breaches of the microvasculature and coagulation effectors [1]. Wound repair is usually characterized by a series of overlapping phases including (1) coagulation, (2) immune response and inflammation, (3) proliferation, and (4) remodeling [2,3]. Keratinocytes (KCs) at the wound edge loosen their adhesion to the basal lamina, creating a

* Corresponding author Department of Hand Surgery & Micro Orthopedics, Luoyang Orthopedic Hospital of Henan Province (Orthopedic Hospital of Henan Province), No. 100, Yongping Road, Guancheng Hui District, Zhengzhou 450016, Henan, PR China.

E-mail address: lyzhao999@163.com (Z. Zhao).

¹ Xiaoling Li and Zhiwei Zhao contributed equally to this study.

<https://doi.org/10.1016/j.heliyon.2024.e26982>

Received 29 October 2023; Received in revised form 19 February 2024; Accepted 22 February 2024

Available online 28 February 2024

2405-8440/© 2024 The Authors. Published by Elsevier Ltd. This is an open access article under the CC BY-NC-ND license (<http://creativecommons.org/licenses/by-nc-nd/4.0/>).

migrating epithelial tongue, and the activation of local microvascular endothelial cells (MECs), which lie on the inner surface of blood vessels, is a necessary step for angiogenesis [4]. Therefore, rat KCs and MECs were used in this study as the *in vitro* models for wound healing.

Panax notoginseng (Burk.) F. H. Chen (Araliaceae), known as Sanchi in East Asian countries, is one of the main herbs in traditional Chinese medicine [5]. *P. notoginseng* was first used by minority ethnic groups in Southwest China and became more widely accepted during the Ming Dynasty to promote blood circulation [6]. *P. notoginseng* has varied biological functions, such as anti-inflammatory effects, antioxidant, and anticancer effects [7]. For instance, the extract of *P. notoginseng* exerts a cardioprotective effect in acute myocardial infarction by enhancing endothelial migration and angiogenesis [8]. More relevantly, 0.1 mM *P. notoginseng* significantly accelerated wound closure in mice with dorsal cutaneous wounds by narrowing the size of lesions and decreasing the formation of scars, which was related to fibroblast accumulation suppression [9]. However, little is known about its regulatory role in KCs and MECs. Hydrogels, available as gels or sheets, are applicable in wounds with an overlying necrotic layer or eschar because they contain highly hydrophilic cross-linked polymers that elevate the moisture content of wounds and improve the autolytic debridement of eschars [10]. Therapeutic compounds are stored in the pores of hydrogels and released into the wound [11]. In this study, we prepared hydrogels with Sanchi extract for *in vivo* treatment to observe the effects of Sanchi on wound healing.

NG-R1, the main active component in Sanchi, has been reported to attenuate synovial inflammation by suppressing the NFκB signaling pathway [12]. Interleukin-1β (IL1B) is a potent pro-inflammatory cytokine that is crucial for host defense responses to infection and injury [13] and is known to activate the NFκB signaling pathway [14]. Based on the findings described above, we aimed to evaluate the effects of Sanchi on KCs and MECs *in vitro* and its therapeutic effects *in vivo* and to dissect the underlying molecular mechanism of the IL1B-mediated NFκB signaling pathway.

2. Materials and methods

2.1. Preparation of the aqueous solution of sanchi extract

Sanchi extract powder (batch number: 2630001) was purchased from Beijing Tong Ren Tang (Beijing, China) and a voucher specimen (21-MDL-0628-SLY) was deposited in the laboratory of the Luoyang Orthopedic Hospital of Henan Province. As previously reported [15], 5 g of Sanchi powder was mixed with 300 mL of water at 18 °C, and the mixture was centrifuged at 4 °C at 8000 × g four times (60 s each time). The supernatant was filtered through a 0.22 μm nylon membrane, sterilized by UV irradiation, and stored at room temperature. HPLC data showed that the supernatant contained 9.1% notoginsenoside R1, 38.4% notoginsenoside Rg1, 29.6% notoginsenoside Rb1, 2.8% notoginsenoside Rd, and 3.7% notoginsenoside Re.

2.2. Preparation of hydrogels containing sanchi

A 5% or 10% (v/v) hydrogel of Sanchi extract was prepared. Hyaluronic acid/gelatin (HA/G) hydrogels were designed as previously described [16,17]. A 15% aqueous gelatin solution was prepared using deionized water and gelatin. The hyaluronic acid solution was prepared using hyaluronic acid and hydrochloric acid solutions. After that, 0.3 g of 1-(3-dimethylaminopropyl)-3-ethylcarbodiimide hydrochloride was added to the solution for 1-h stirring. The solution was adjusted to pH = 4.7 using 0.1 M HCL. Two 5-mL syringes were used to draw 5 mL of gelatin solution and 5 mL of hyaluronic acid solution, and different volumes of Sanchi solution were added and mixed to obtain hydrogels containing Sanchi. Hydrogels without the Sanchi solution were used as controls.

2.3. Rheological analysis

The rheological properties of the HA/G hydrogels were characterized using an MCR 302e rheometer (Anton Paar GmbH, Austria) equipped with a parallel plate system. In the oscillation mode, 200 μL of preactivated NHS solution (130672, Merck Millipore, Darmstadt, Germany) was mixed with an equal volume of gelatin solution in a mixing chamber at 37 °C using a double syringe. The mixed solution was then applied to the bottom plate, and the top plate was lowered and kept a gap of 0.7 mm to the bottom plate. The storage modulus G' and loss modulus G'' of the material were subsequently measured at a 10% strain and an oscillation frequency of 1 Hz. The gelation time was defined as the point at which the value of the storage modulus exceeded the loss modulus [18].

2.4. Thermal stability and protein hydrolytic degradation

First, 1 mL of hydrogel was prepared in a cell culture dish and left overnight, followed by incubation of the hydrogel at 37 °C in PBS solution at pH 7.4 to check for thermal stability.

Protein hydrolytic degradability was tested by incubating the hydrogels in 0.25% trypsin-EDTA (T3924; Merck Millipore) at room temperature. After warming for 0, 5, 10, 15, 20, 30, 60, 120, or 240 min, the hydrogels were washed with deionized water at various time points, air-dried, and weighed at room temperature (Wt). The remaining weight percentage (W%) of the hydrogel at each time point was calculated using the following formula: $W\% = Wt/W0 \times 100\%$, where W0 is the dry weight of each hydrogel without any treatment.

2.5. Animals

Eight-week-old male Sprague–Dawley rats (280 ± 30 g) were purchased from Hunan SJA Laboratory Animal Co., Ltd. (Changsha, Hunan, China) and housed under standard environmental conditions (22 ± 2 °C, 55–60% relative humidity, and 12 h light/dark cycle) with free access to water and food. All rats were acclimated for at least seven days before the experiments. All processes involving rats were authorized by the Animal Research Ethics Committee of Luoyang Orthopedic Hospital of Henan Province (Orthopedic Hospital of Henan Province) (approval number: MDL2021-12-13-01).

Rats were anesthetized by intraperitoneal injection of ketamine (100 mg/kg) and xylazine (10 mg/kg), followed by skin preparation and disinfection with iodine. A 1.2-cm-diameter full-length wound was made on the dorsal surface of the rats using a biopsy punch. The rats were then divided into six groups ($n = 6$): Control (no other treatment), Hydrogel (treated with hydrogel without Sanchi), 5% Hydrogel (treated with a hydrogel containing 5% Sanchi), 10% hydrogel (treated with a hydrogel containing 10% Sanchi), 10% Hydrogel + a recombinant adenovirus type-5 (Ad5)-NC (treated with a hydrogel containing 10% Sanchi and Ad5-NC), 10% Hydrogel + Ad5-IL1B (treated with a hydrogel containing 10% Sanchi and Ad5-IL1B). The wound closure rate was calculated using the formula: wound healing rate = $(S0-SA)/S0 \times 100\%$, where S0 represents the original wound area on day 0, and SA represents the wound area on day A [19,20].

IL1B overexpressing adenovirus (pAV[Exp]-EGFP-CMV > rll1b [NM_031512.2]) based on the mammalian gene expression Ad5 adenovirus vector was purchased from VectorBuilder (Guangzhou, Guangdong, China). The empty adenovirus vector (Ad5-NC) was used as a control. The viral titer was 10^{10} IFU/mL, and 100 μ L of adenovirus was injected into the wound margin tissues of each rat. On day 10, all rats were euthanized by intraperitoneal injection of 150 mg/kg sodium pentobarbital, and skin tissues were harvested from the wound edges. One part of the tissue was paraffin-embedded and the other part was cryopreserved.

2.6. Histological examination

Paraffin-embedded skin wound tissues were sectioned at 4 μ M. After routine dewaxing and hydration, inflammatory infiltration and collagen deposition in the tissues were detected using a hematoxylin-eosin (HE) staining kit (G1120; Beijing Solarbio Life Sciences Co., Ltd., Beijing, China) and Masson's trichrome stain kit (G1340; Solarbio), respectively, according to the manufacturer's protocol. For Masson's trichrome staining, the area of blue collagen deposition was quantified using ImageJ software.

2.7. Immunohistochemistry

The sections were incubated with 3% H₂O₂ for 10 min at room temperature to block endogenous peroxidase activity, followed by heat-mediated antigen retrieval using a sodium citrate buffer. The sections were sealed for 60 min at room temperature using 5% normal goat serum and incubated with diluted primary antibodies against IL-1B (1:200, ab283822, Abcam, Cambridge, UK), Phospho-NF- κ B p65 (Ser536) (1:200, GTX55114, GeneTex, Inc., Alton Pkwy Irvine, CA, USA), and CD31 (1:2000, ab182981, Abcam) at 4 °C overnight, followed by incubation with goat anti-rabbit horseradish peroxidase (HRP)-conjugated IgG H&L (1:2000, ab6721, Abcam) for 1 h at room temperature. Color development was performed using diaminobenzidine, and counter-staining was performed using hematoxylin. The positive signal of the staining (tan color) was quantified using ImageJ software.

2.8. Cell culture

Rat KCs (CP-R094) and rat MECs (CP-R196) were purchased from Procell (Wuhan, Hubei, China) and cultured at 37 °C in 5% CO₂ in epidermal KC complete medium (CM-R094, Procell) and dermal MEC complete medium (CM-R196, Procell), respectively.

The cells were treated with different concentrations of H₂O₂ for 24 h to induce cell damage. The overexpressed DNA plasmid oe-IL1B and the control plasmid oe-NC used for cell transfection were purchased from VectorBuilder, and all transfections were performed using Lipofectamine 3000, according to the manufacturer's protocol.

2.9. Assessment of biochemical indexes

Factors in the tissue supernatants or cell lysates were assayed using the rat IL-6 ELISA kit (ab234570, Abcam), rat TNF alpha ELISA kit (ab100785, Abcam), rat Superoxide Dismutase 1 (SOD1) ELISA kit (E4584, BioVision, Inc., Exton, PA, USA), and rat VEGF ELISA kit (ab100787, Abcam) according to the manufacturer's protocol. Malondialdehyde (MDA) levels in tissue supernatants or cell lysates were measured using the Lipid Peroxidation (MDA) Fluorescence Assay Kit (ab118970, Abcam, Ex/Em 532/553 nm).

2.10. Quantitative polymerase chain reaction (qPCR) assay

Total RNA from cells or tissues was extracted using TRIzol (Beyotime Biotechnology Co., Ltd., Shanghai, China) and reverse-transcribed into cDNA using the BeyoRT™ II cDNA Synthesis Kit (Beyotime). The relative expression of IL1B was measured by qPCR on an Applied Biosystems StepOnePlus Real-Time PCR System (Thermo Fisher Scientific Inc., Waltham, MA, USA) using TB Green Premix Ex Taq (Takara Biotechnology Ltd., Dalian, Liaoning, China). Data were analyzed using the $2^{-\Delta\Delta CT}$ method, and the relative gene expression was normalized to glyceraldehyde-3-phosphate dehydrogenase (GAPDH). The primer sequences used were as follows: IL1B (forward: 5'-TTGAGTCTGCACAGTTCCCC-3'; reverse: 5'-GTCCTGGGAAGGCATTAGG-3') and GAPDH (forward: 5'-

GCATCTTCTTGTGCAGTGCC-3'); reverse: 5'-GATGGTGATGGGTTTCCCGT-3').

2.11. Protein extraction, Western blot analysis, and antibodies

The total protein in the cells was extracted using RIPA lysis buffer and quantified using the BCA Protein Quantification Kit (Yeasen Biotechnology Co., Ltd., Shanghai, China). Medium amounts of proteins were prepared, separated by 12% sodium dodecyl sulfate-polyacrylamide gel electrophoresis, and then transferred to a nitrocellulose membrane. The membranes were blocked in 5% bovine serum albumin solution at room temperature for 1 h and incubated overnight at 4 °C with primary antibodies specific for IL1B (1:1000,

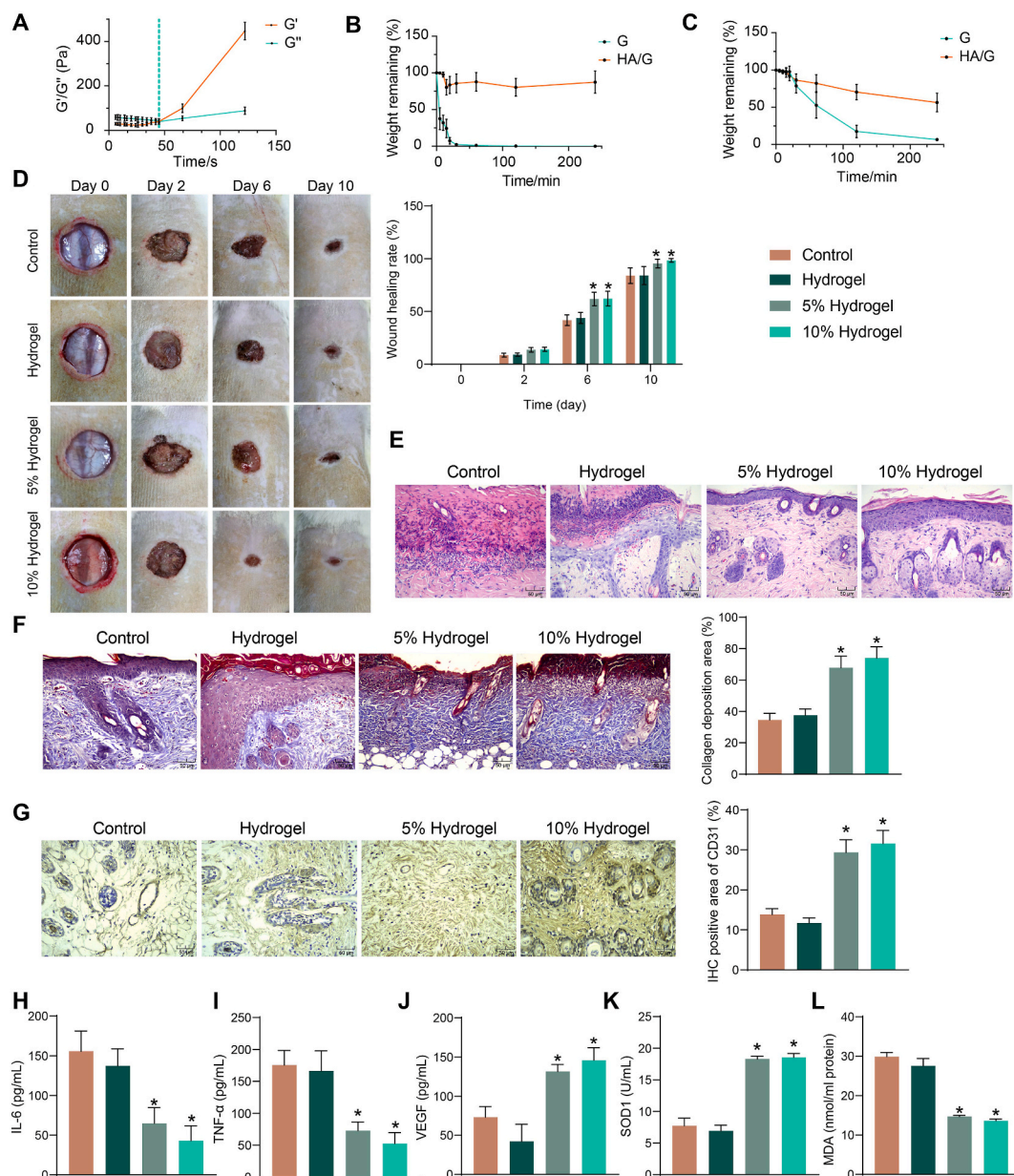


Fig. 1. Sanchi accelerates wound healing in rats. (A) Rheological analysis of HG/A hydrogels. (B) Thermal stability evaluation of HG/A and G hydrogels. (C) Proteolytic degradation stability assessment of HG/A and G hydrogels. (D) Hydrogel containing different concentrations of Sanchi was used to treat the injured rats and to observe the process of wound healing. (E) The inflammatory infiltration in wound tissues in rats was examined using HE staining. (F) Collagen fiber deposition in wound tissues in rats was examined using Masson's staining. (G) Immunohistochemical detection of angiogenic marker CD31 expression in wound tissues in rats. (H–K) The levels of IL-6, TNF- α , VEGF, and SOD1 in wound tissues in rats were examined using ELISA. (L) Analysis of MDA in wound tissues of rats by combining fluorescence with colorimetry. All values are presented as mean \pm SD; n = 6. * p < 0.05. A one-way (F–L) or two-way (D) analysis of variance with Tukey's post hoc test was used for multiple comparisons.

NBP1-42767, Novus Biological Inc., Littleton, CO, USA), phospho-NF- κ B p65 (Ser536) (1:2000, GTX55114, GeneTex), NF- κ B p65 (1:2000, #8242, Cell Signaling Technologies, Beverly, MA, USA), and GAPDH (1:1000, #2118, Cell Signaling Technologies). The membranes were then incubated with HRP-conjugated goat anti-rabbit IgG H&L secondary antibody (1:5000, ab6721, Abcam) for 1 h at room temperature and developed using an ECL reagent (Abcam). ImageJ software was used to quantify protein band densities. The densities of individual protein bands were normalized to those of the corresponding GAPDH band.

2.12. Methyl thiazolyl tetrazolium (MTT) assay

MECs and KCs were seeded into 96-well plates at 5000 cells per well. Specific treatments were performed according to experimental requirements. Subsequently, 10 μ L of MTT solution (Dojindo Laboratories, Kumamoto, Japan) was added to each well for 4-h co-culture and then replaced with 100 μ L dimethyl sulfoxide (DMSO). After another 3–4 h of incubation at 37 °C, the formazan was solubilized. The optical density (OD) of each well was measured at 570 nm to determine cell viability.

2.13. Terminal deoxynucleotidyl transferase-mediated dUTP nick end-labeling (TUNEL)

Apoptosis was measured using a one-step TUNEL Apoptosis Assay Kit (Beyotime). Treated KCs or MECs in 96-well plates were fixed with 4% paraformaldehyde for 30 min and then permeabilized in 0.3% Triton X-100 for 5 min. The cells were incubated with the TUNEL assay solution for 60 min at 37 °C in the dark. After nuclear staining with 4',6-diamidino-2-phenylindole, confocal fluorescence microscopy was used to capture fluorescent images. The apoptosis rate was evaluated as the percentage of TUNEL-positive cells (green) relative to the total number of cells.

2.14. Tube formation assay

A tube formation assay was used to test the angiogenic potential of the MECs. The 96-well plates were pre-coated with 50 μ L of Ceturegel™ Matrix LDEV-Free substrate gel (Yeasen) and polymerized at 37 °C for 30 min. Treated MECs were seeded into each well of a 96-well plate at a density of 1×10^5 cells/well. After 24 h, the tube formation was observed under an inverted optical microscope (Carl Zeiss, Oberkochen, Germany). The photographed angiogenic images were analyzed using AngioTool (Version 0.6a) [21]. AngioTool automatically identifies the vessel contours and presents the quantitative results as “Vessels area (%)”, which is automatically calculated by the parameter “Vessels area/Explant area \times 100%”.

2.15. Dual-luciferase assay

The NF- κ B luciferase reporter plasmid (Yeasen) was used to detect the NF κ B pathway activity. Briefly, the above reporter plasmids were transfected into MECs and KCs using Lipofectamin3000 with oe-NC or oe-IL1B, respectively. Cells not transfected with plasmids served as controls. Subsequent H₂O₂ exposure was performed or not. Forty-eight hours after treatment, activation of the NF κ B pathway was measured by assaying luciferase activity using the Dual-Luciferase Reporter Gene Assay Kit (Yeasen).

2.16. Statistics

Data are expressed as means \pm standard deviation (SD). Each experiment was repeated at least thrice. All statistical analyses were performed using GraphPad Prism 8.0 (GraphPad Software, San Diego, CA, USA). The Shapiro-Wilk test was used as the normality test. Data were evaluated using unpaired *t*-tests. One-way or two-way analysis of variance (ANOVA) with Tukey's *post-hoc* test was used for multiple comparisons. Statistical significance was indicated by a *p*-value of <0.05 .

3. Results

3.1. Sanchi accelerates the healing of mechanical skin injuries

We prepared hydrogels without Sanchi (0%) extract or containing 5% or 10% Sanchi extract, to treat rats with skin trauma. We first analyzed the physical properties of the hydrogels, and the results of the rheological analysis showed that the crossover point of the energy storage modulus (G') and loss modulus (G'') of the HA/G hydrogels was 45 s, indicating the time at which the mixture changed from a viscous solution to a hydrogel (Fig. 1A). By comparing the thermal stability and protein hydrolytic degradation with G hydrogel, it was found that the chemically cross-linked HA/G hydrogel was stable and heat-resistant (Fig. 1B). Similarly, the stability of the HA/G hydrogel against protein hydrolytic degradation was significantly higher than that of the G hydrogel (Fig. 1C).

Subsequently, we treated the rats with wounds using HA/G hydrogels, we found that Hydrogels without Sanchi extract did not show beneficial effects on wound healing, whereas hydrogels containing 5% or 10% Sanchi extract significantly promoted wound healing (Fig. 1D). We observed by HE staining that Sanchi extracts also significantly reduced inflammatory cell infiltration in the wound skin tissues (Fig. 1E), while Masson staining showed that collagen fiber deposition in the wound margin tissues was significantly enhanced by Sanchi (Fig. 1F). Immunohistochemistry revealed a significant increase in the angiogenic marker CD31 in the Sanchi-treated groups (Fig. 1G). By analyzing the levels of oxidative stress markers and inflammatory factors in tissues, we observed that Sanchi extracts significantly reduced the levels of IL-6, TNF- α , and MDA and increased the levels of SOD1 and VEGF in wound

tissues (Fig. 1H-L).

3.2. Sanchi inhibits H_2O_2 -induced inflammatory cell injury

We detected the promoting effect of Sanchi on wound healing *in vivo* and subsequently analyzed the impact of Sanchi *in vitro*. First, we simulated inflammatory cell injury by treating KCs with graded concentrations of H_2O_2 for 24 h. Given that Sanchi has a facilitative effect on angiogenesis, MECs have also been used for *in vitro* experiments. Cell damage was measured by the MTT assay (Fig. 2A and B). Both cell lines exhibited dose-dependent damage, and H_2O_2 at 60 μM caused significantly inhibited the viability of both cell lines. By the time the concentration reached 100 μM , the viability of both cell types was reduced by more than half. Therefore, a concentration of 100 μM was selected for subsequent experiments.

Sanchi was then used to treat the H_2O_2 -induced cells. Sanchi significantly attenuated H_2O_2 -induced cell damage and improved cell viability, and Sanchi had a more outstanding effect on saving the viability of KCs (Fig. 2C). The results of the TUNEL assays showed that H_2O_2 induced apoptosis of KCs and MECs by over 20%. In contrast, Sanchi treatment partially reduced apoptosis in KCs and MECs (Fig. 2D). ELISA was performed to assess the release of pro-inflammatory factors in the cell supernatant. H_2O_2 induced the release of IL-6 and TNF- α from the cells, while Sanchi exhibited an inhibitory effect on the inflammatory response, as evidenced by lower IL-6 and TNF- α concentrations (Fig. 2E and F). H_2O_2 also contributed to an increase in MDA content and a decrease in SOD content in cells, while Sanchi reduced the MDA content and increased SOD content in cells (Fig. 2G and H). Further studies found that H_2O_2 significantly inhibited the angiogenic ability of MECs and narrowed the area covered by blood vessels, whereas Sanchi treatment promoted the angiogenic effect (Fig. 2I).

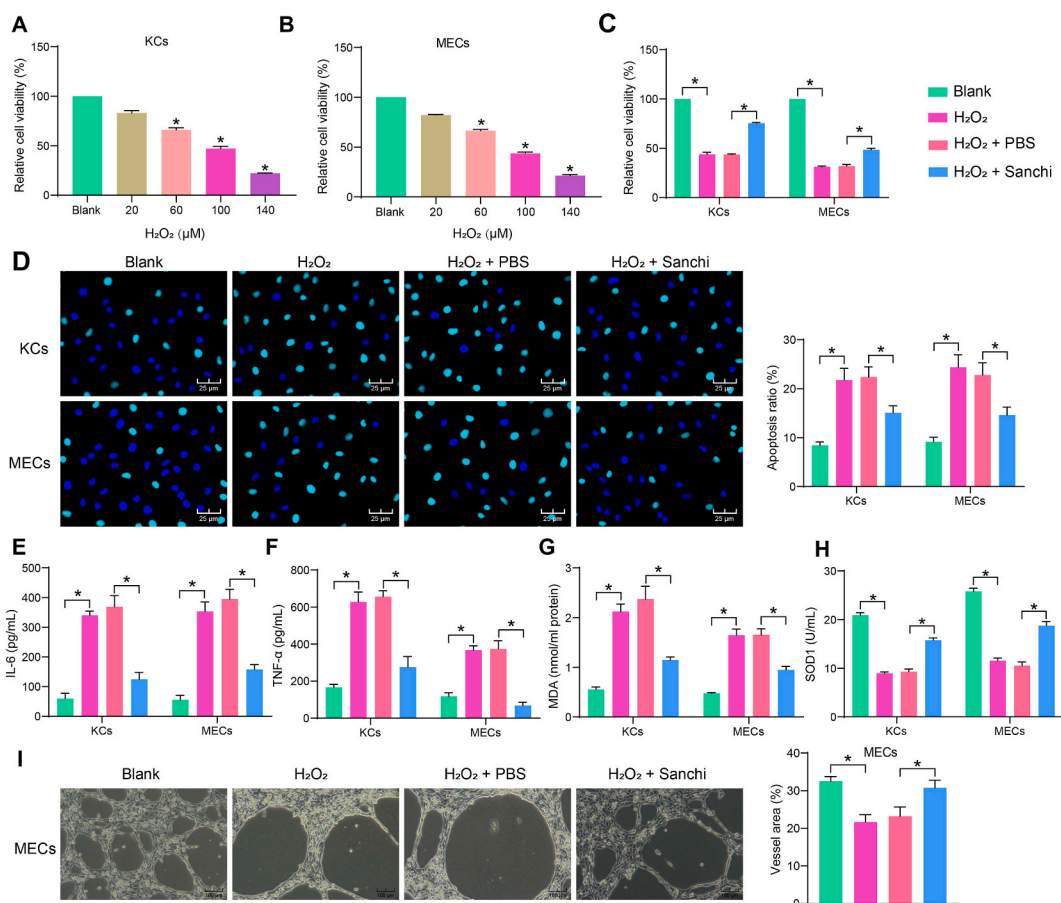


Fig. 2. Sanchi restores the viability potential and reduces inflammatory and oxidative stress response of KCs and MECs. (A–B) Effect of different concentrations of H_2O_2 treatment on cell damage in KCs (A) and MECs (B) by MTT assay. (C) Effect of Sanchi against H_2O_2 -induced impairment of cell viability in KCs and MECs by MTT assay. (D) Effect of Sanchi on H_2O_2 -induced apoptosis in KCs and MECs by TUNEL assay. (E–F) Effect of Sanchi on IL-6 (E) and TNF- α (F) content in KCs and MECs by ELISA. (G) Effect of Sanchi on MDA in KCs and MECs by combining fluorescence with colorimetry. (H) Effect of Sanchi on SOD1 content in KCs and MECs by ELISA. (I) Effect of Sanchi on the angiogenic capacity of H_2O_2 -induced MECs by tube formation assay. All values are presented as mean \pm SD from three independent experiments. * $p < 0.05$. A one-way (A, B, I) or two-way (C–H) analysis of variance with Tukey's post hoc test was used for multiple comparisons.

3.3. IL1B is a downstream target candidate of sanchi

To clarify the specific mechanism of Sanchi for wound healing, we first downloaded the related gene targets of Sanchi (herb ID: HERB004783) from Herb: A high-throughput experiment- and reference-guided database of traditional Chinese medicine (<http://herb.ac.cn/>), and performed KEGG pathway enrichment analysis (Fig. 3A). The results showed that Sanchi mainly affected inflammation-related pathways, including the NFκB signaling pathway (KEGG ID: hsa04064), which is consistent with its inhibitory effects on inflammatory damage. Among target genes of Sanchi (PTGS2, BCL2, TNF, CXCL8, NFKBIA, RELA, PRKCB, IL1B, and IRAK4) that are enriched to NFκB signaling pathway, IL1B is the primary driver signal to activate NFκB signaling pathway and subsequent inflammation response (Fig. 3B). Therefore, we chose IL1B as a key downstream target of Sanchi for our analysis.

By RT-qPCR, we detected that Sanchi treatment reduced IL1B mRNA expression in rat wound tissues (Fig. 3C). Consistently, immunohistochemical staining showed Sanchi treatment also resulted in a significant reduction in IL1B and p-NFκB expression in wound tissues (Fig. 3D and E).

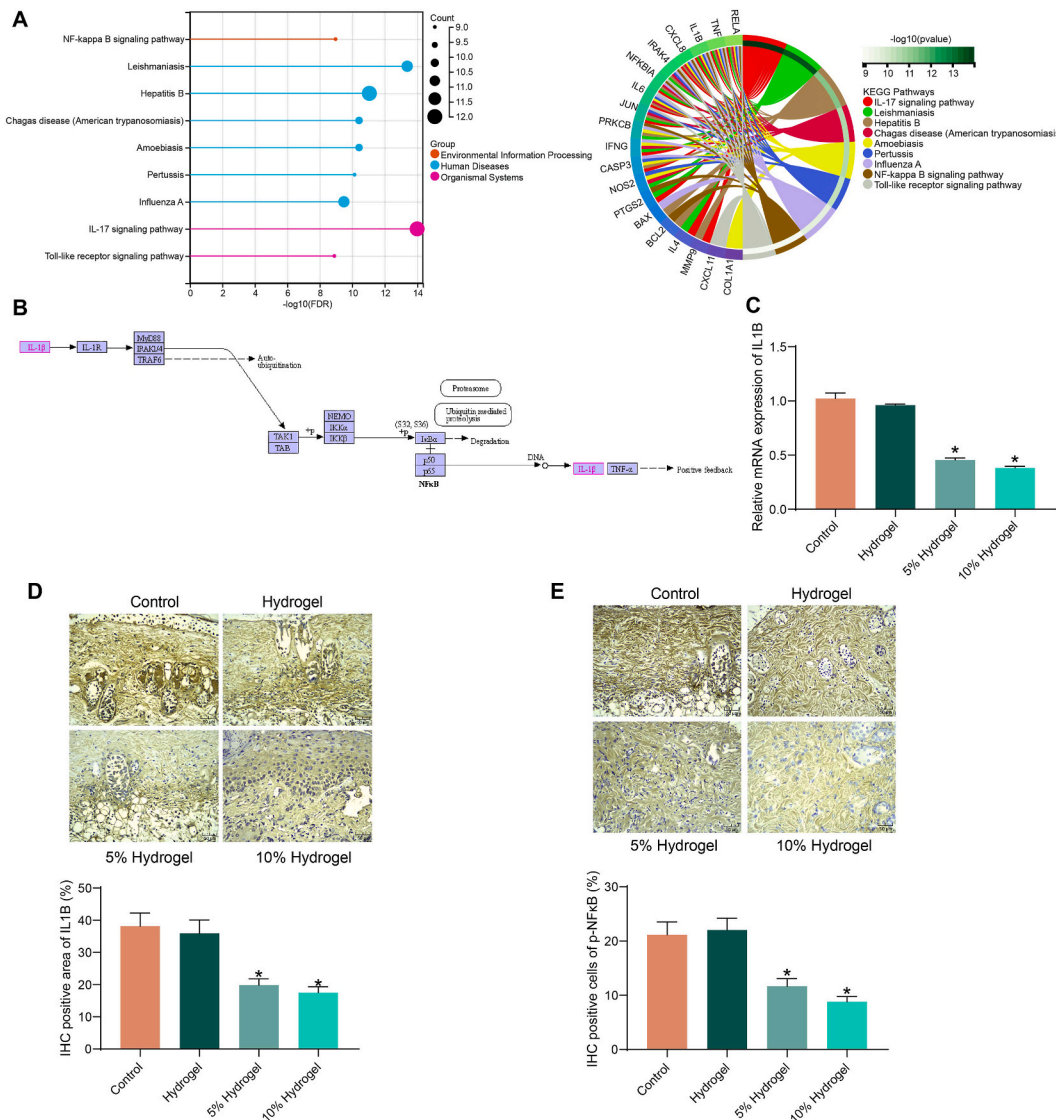


Fig. 3. Sanchi inhibits the expression of IL1B. (A) The pathways affected by Sanchi-targeted genes using KEGG pathway enrichment analysis. (B) The position of IL1B in the NFκB signaling pathway. (C) IL1B mRNA expression in rat wound tissues using RT-qPCR. (D–E) Protein expression of IL1B (D) and p-NFκB (E) in rat wound tissues using immunohistochemical staining. All values are presented as mean ± SD; n = 6. *p < 0.05. A one-way (C–E) analysis of variance with Tukey’s post hoc test was used for multiple comparisons.

3.4. Sanchi-mediated suppression of IL1B expression leads to NFκB pathway deficit

We further analyzed the regulatory effects of Sanchi on the NFκB pathway *in vitro*. We detected by Western blot that H₂O₂ treatment increased IL1B expression and the extent of NFκB phosphorylation in both KCs and MECs, whereas Sanchi treatment inhibited IL1B expression and the extent of NFκB phosphorylation (Fig. 4A and B). NFκB pathway activity was detected by NFκB luciferase reporter plasmid (Fig. 4C). We found that H₂O₂ induced the activation of the NFκB pathway in both cell lines, while Sanchi specifically inhibited the H₂O₂-induced activation of this pathway (Fig. 4D).

We transfected the overexpression DNA plasmid of IL1B into Sanchi-treated cells and detected the overexpression efficiency by RT-qPCR (Fig. 4E). Western blot showed that restoration of IL1B contributed to NFκB phosphorylation in both cell lines (Fig. 4F and G), and the NFκB pathway was reactivated (Fig. 4H). This suggests that the impairment of the NFκB pathway by Sanchi is achieved through the inhibition of IL1B.

3.5. The protective effect of sanchi on inflammatory cell injury is reversed by IL1B

By MTT assay, we detected that overexpression of IL1B led to significant mitigation of the protective effect of Sanchi against H₂O₂-induced damage in KCs and MECs (Fig. 5A) and a promotion in the apoptotic rate of cells (Fig. 5B), accompanied by an elevation in the levels of IL-6, TNF-α and MDA (Fig. 5C–E). By contrast, the levels of SOD1 in cells were significantly reduced (Fig. 5F). Meanwhile, the

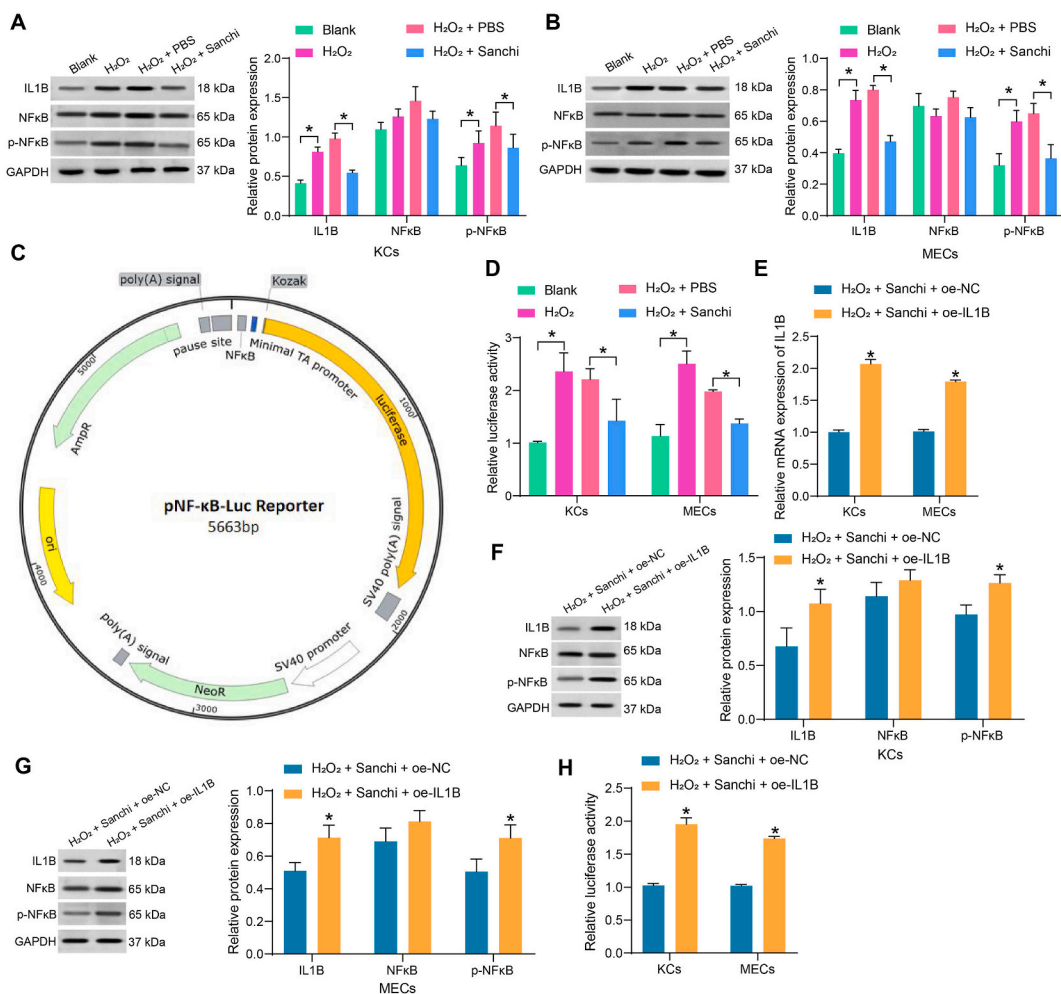


Fig. 4. Sanchi promotes wound healing by blocking the IL1B-mediated NFκB pathway. (A–B) The effects of H₂O₂ treatment and Sanchi treatment on IL1B expression and the extent of NFκB phosphorylation in KCs (A) and MECs (B) using Western blot assays (full, non-adjusted blots are provided in supplementary material). (C) The mapping of NF-κB luciferase reporter plasmid. (D) The effect of H₂O₂ treatment and Sanchi treatment on NFκB pathway activity using dual-luciferase assay. (E) Overexpression efficiency of oe-IL1B using RT-qPCR. (F–G) The effect of oe-IL1B on IL1B expression and NFκB phosphorylation in KCs (F) and MECs (G) using Western blot assays (full, non-adjusted blots are provided in supplementary material). (H) The effect of oe-IL1B on NFκB pathway activity using dual-luciferase assay. All values are presented as mean ± SD from three independent experiments. **p* < 0.05. A two-way (A–G) analysis of variance with Tukey's post hoc test was used for multiple comparisons.

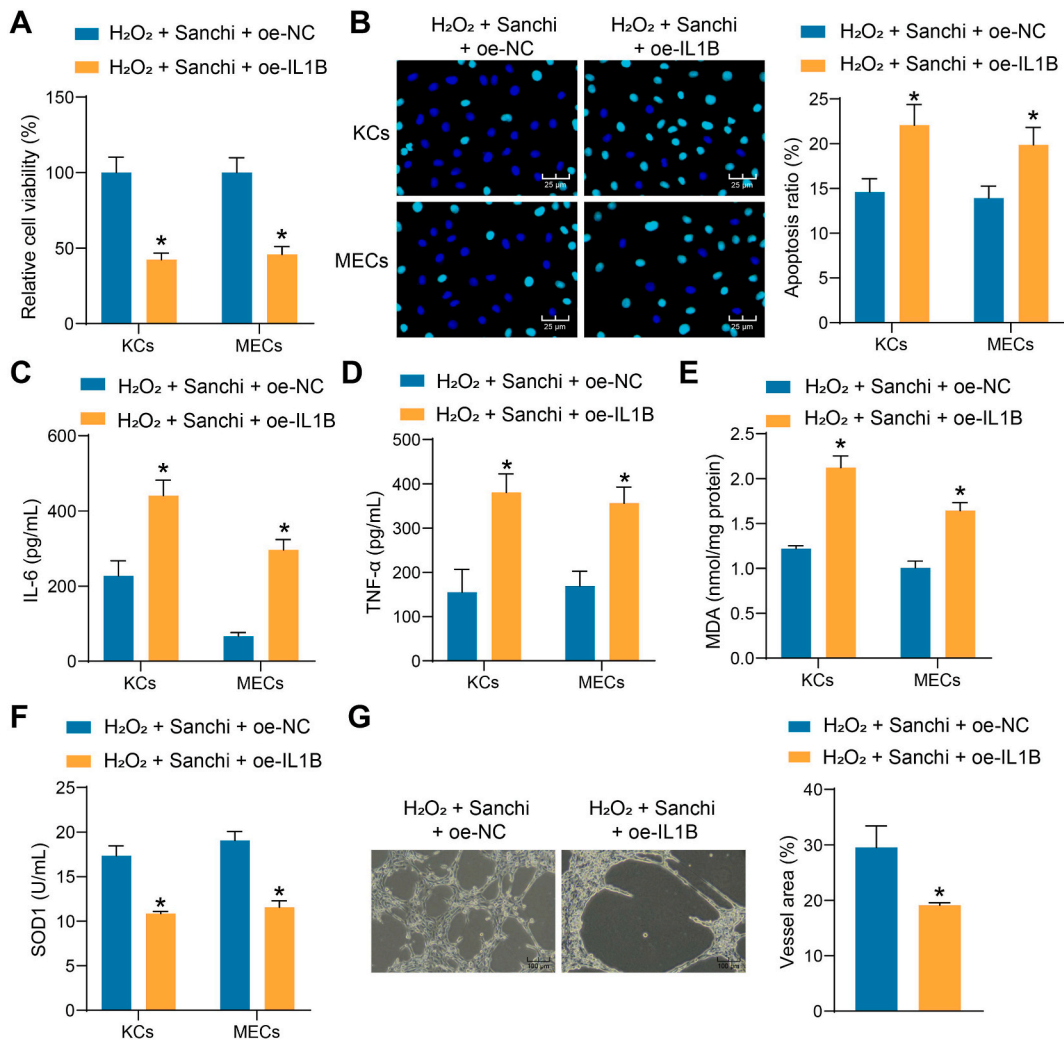


Fig. 5. Overexpression of IL1B mitigates the protective effect of Sanchi on KCs and MECs. (A) Effect of oe-IL1B against H₂O₂-induced impairment of cell viability in KCs and MECs by MTT assay. (B) Effect of oe-IL1B on H₂O₂-induced apoptosis in KCs and MECs by TUNEL assay. (C–D) Effect of oe-IL1B on IL-6 (C) and TNF-α (D) content in KCs and MECs by ELISA. (E) Effect of oe-IL1B on MDA in KCs and MECs by combining fluorescence with colorimetry. (F) Effect of oe-IL1B on SOD1 content in KCs and MECs by ELISA. (G) Effect of oe-IL1B on the angiogenic capacity of H₂O₂-induced MECs by tube formation assay. All values are presented as mean ± SD from three independent experiments. **p* < 0.05. An unpaired *t*-test (G) or two-way (A–F) analysis of variance with Tukey's post hoc test was used for multiple comparisons.

angiogenic capacity of MECs was significantly reduced after overexpression of IL1B (Fig. 5G).

3.6. IL1B inhibits the promoting effects of sanchi on wound healing

Rescue experiments were performed using overexpression adenovirus of IL1B with 10% Sanchi hydrogel. We found that the combined use of Ad5-IL1B resulted in a curbed wound-healing process (Fig. 6A). Ad5-IL1B successfully increased IL1B expression and *p*-NFκB expression in rat wound tissues, as revealed by immunohistochemical staining (Fig. 6B and C). The angiogenic marker CD31 was also significantly reduced in wound tissues after overexpression of IL1B (Fig. 6D). It was found by HE staining that Ad5-IL1B treatment led to an increase in inflammatory cell infiltration in the wound tissues (Fig. 6E). The results of the ELISA assay showed that IL-6, TNF-α, and MDA contents in wound tissues increased significantly after overexpression of IL1B, and SOD1 content was decreased in tissues (Fig. 6F–I). Meanwhile, the upregulation of IL1B resulted in a significant decrease in VEGF content (Fig. 6J). Finally, Masson's staining showed that collagen deposition in the wound tissues was also significantly inhibited by overexpression of IL1B (Fig. 6K).

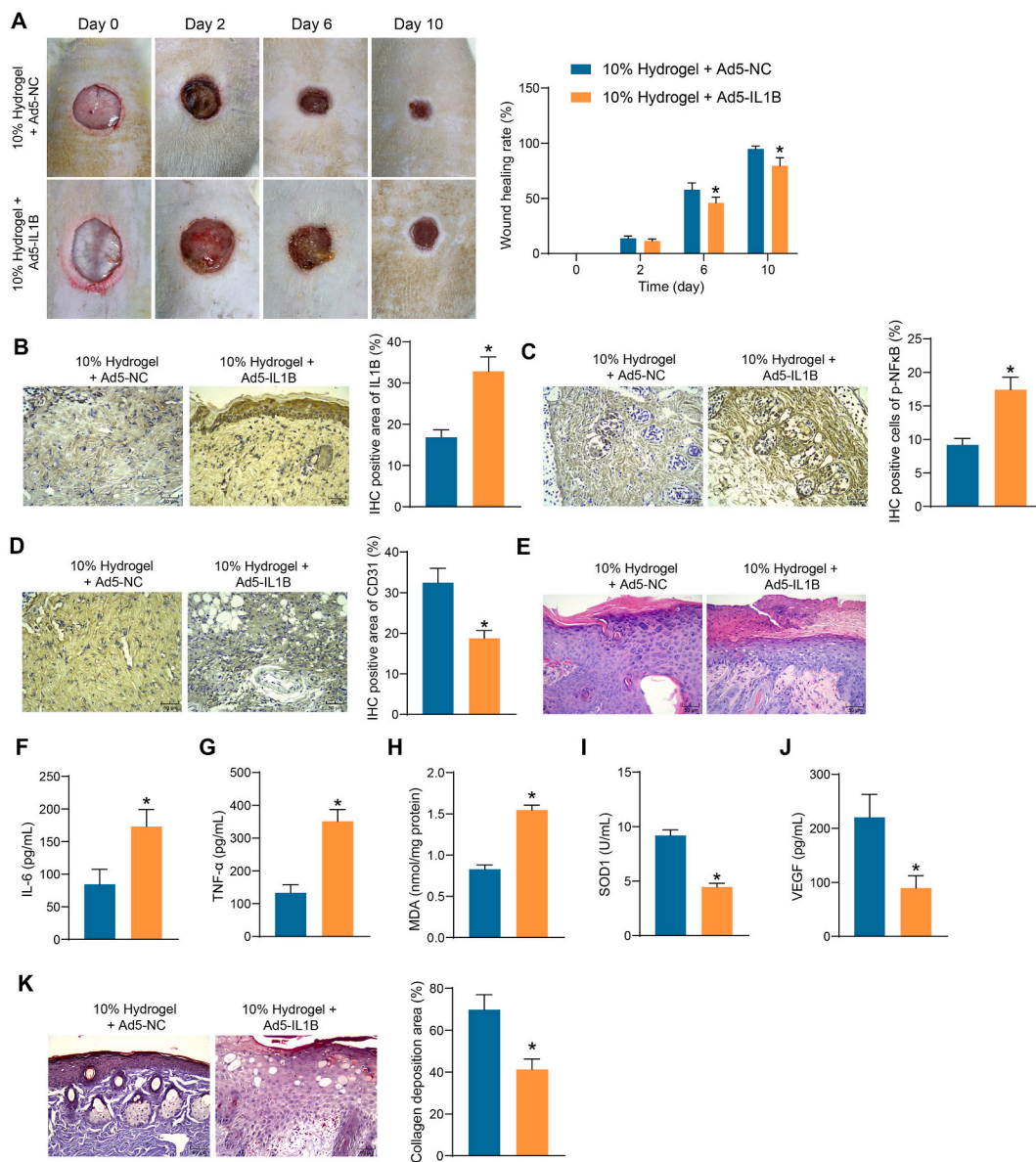


Fig. 6. Overexpression of IL1B mitigates the promoting effects of Sanchi on wound healing. (A) Wounded rats were treated with IL1B overexpression adenovirus combined with a hydrogel containing 10% Sanchi to observe the process of wound healing. (B–D) Immunohistochemical detection of IL1B (B), p-NFκB (C), and CD31 (D) in wound tissues in rats. (E) The inflammatory infiltration in wound tissues in rats was examined using HE staining. (F–G) The levels of IL-6 (F) and TNF-α (G) in wound tissues in rats were examined using ELISA. (H) Analysis of MDA in wound tissues of rats by combining fluorescence with colorimetry. (I–J) The levels of SOD1 (I) and VEGF (J) in wound tissues in rats were examined using ELISA. (K) Collagen fiber deposition in wound tissues in rats was examined using Masson's staining. All values are presented as mean ± SD; n = 6. * $p < 0.05$. An unpaired t-test (B–K) or two-way (A) analysis of variance with Tukey's post hoc test was used for multiple comparisons.

4. Discussion

Unhealed wound is a serious public problem, which brings economic burdens and psychological pressure to patients, and various herbal drugs in traditional Chinese medicine have been applied for wound healing since ancient times [22]. Herein, we successfully prepared hydrogel containing Sanchi extract capable of promoting wound healing in a rat model. In addition, Sanchi restored the viability potential and reduced the inflammatory response and oxidative stress of KCs and MECs. When examining the biomolecules involved using bioinformatics tools, we found that Sanchi impaired the NFκB pathway activation by lowering the expression of IL1B. Overexpression of IL1B overturned the effects of Sanchi *in vivo* and *in vitro* by activating the NFκB pathway.

P. notoginseng has been revealed to restrain hypertrophic scar formation by suppressing cell migration and boosting apoptosis and G1 arrest of hypertrophic scar fibroblasts [23]. Ginsenoside Rb1, a monomeric active constituent extracted from *P. notoginseng*, has

been verified to decrease the scab removal time and fur growth time while increasing the wound healing rate in rats [24]. Subsequently, we sought to decipher the mechanism for the role of Sanchi in wound healing. It has been reported that overexposure to oxidative stress leads to impaired wound healing, and antioxidants are thus postulated to accelerate wound healing [25]. In addition, the microenvironment of a chronic wound is characterized by the accumulation of inflammatory cytokines, such as TNF- α and IL-6, and an abundance of reactive oxygen species [26]. Therefore, we examined the levels of pro-inflammatory factors TNF- α and IL-6 as well as oxidative stress markers MDA and SOD1. It was found that Sanchi extract alleviated the inflammatory responses and oxidative stress in the wound tissues of rats. VEGF family can initiate the process of wound healing by promoting early angiogenesis and the migration of endothelial cells [27]. When endothelial cells begin to transition, intermediate phenotypes occur and proceed with the loss of endothelial markers like CD31, which stands for primarily junctional protein maintaining the endothelial layer integrity [28]. Here, we also observed that Sanchi treatment significantly boosted the expression of CD31 and VEGF in the wound tissues of rats.

Second, we assessed whether these *in vivo* findings can be reproduced *in vitro*. Endothelial cells play an important role in the cutaneous immune system by recruiting inflammatory cells to the skin and inducing the release of cytokines and chemokines [29]. KCs represent an ideal cell model for the wound healing assay because they are involved in both oxidative stress and inflammation of the wound healing process [30,31]. *P. notoginseng* has been reported to promote tube formation in human umbilical vein endothelial cells [32], but its effects on KCs and MECs remain largely unexplored. Our *in vitro* evidence suggested that the suppressive effects of H₂O₂ on KCs and MECs viability were partially restored by Sanchi extract. In addition, the inflammatory responses and oxidative stress in these two cell lines were mitigated by Sanchi as well.

To further illustrate the mechanisms that were involved in the promoting effects of Sanchi on wound healing, we conducted bioinformatics analyses. IL1B-mediated NF κ B pathway attracted our attention. In a recent review, the NF κ B pathway has been summarized as one of the pathways regulated by Traditional Chinese medicine that are capable of maintaining inflammatory interaction balance and suppressing oxidative stress during diabetic wound healing [33]. Elevated levels of IL1B have been identified in samples from diabetic patients when compared to normal wound tissues, and IL1B at high concentrations inhibited fibroblast proliferation and migration by inducing p38 phosphorylation and the ensuing p38 MAPK pathway [34]. To determine that the NF κ B pathway is indeed a downstream effector of IL1B in the present study, we conducted rescue experiments using overexpression DNA plasmid of IL1B *in vitro* and IL1B overexpression adenovirus *in vivo*. As expected, the upregulation of IL1B reactivated the NF κ B pathway in two cell lines and wound tissues of rats, thereby overturning the effects of Sanchi on wound healing.

Hydrogels (whether injectable or dressing) have been implicated in the biomedical field because of antimicrobial properties, adhesion and hemostasis, anti-inflammatory and anti-oxidation, substance delivery, stimulus-response, and conductivity [35–37]. In addition, hydrogels containing fibrin-collagen and topical erythropoietin have been applied in diabetic patients with no treatment-related adverse events [38,39]. Clinical trials on our included patients are still needed to verify the safety of Sanchi-containing hydrogels.

5. Conclusions

Taken together, according to the results of *in vitro* and *in vivo* assays, we found that Sanchi might be a promising therapy to repair skin wounds by alleviating inflammation and oxidative stress and promoting KC viability and MEC angiogenesis. We have advanced current knowledge regarding the mechanisms of Sanchi in wound healing, indicating that hydrogel containing Sanchi could be an option for clinical wound care.

Data availability statement

The datasets used and/or analyzed during the current study are available from the corresponding author upon reasonable request.

Funding

The authors reported there is no funding associated with the work featured in this article.

Ethical approval

All processes involving rats were authorized by the Animal Research Ethics Committee of Luoyang Orthopedic Hospital of Henan Province (Orthopedic Hospital of Henan Province) (approval number: MDL2021-12-13-01). Animal studies were performed in compliance with the ARRIVE guidelines. All animals received humane care according to the National Institutes of Health (USA) guidelines.

CRedit authorship contribution statement

Xiaoling Li: Writing – original draft, Validation, Project administration, Formal analysis, Data curation, Conceptualization. **Zhiwei Zhao:** Writing – original draft, Validation, Project administration, Investigation, Formal analysis, Conceptualization. **Bo Cui:** Writing – review & editing, Supervision, Resources, Methodology, Formal analysis, Data curation. **Yanfeng Li:** Writing – review & editing, Supervision, Software, Investigation, Formal analysis, Data curation.

Declaration of competing interest

The authors declare that they have no known competing financial interests or personal relationships that could have appeared to influence the work reported in this paper.

Appendix A. Supplementary data

Supplementary data to this article can be found online at <https://doi.org/10.1016/j.heliyon.2024.e26982>.

References

- [1] O. Garraud, W.N. Hozzein, G. Badr, Wound healing: time to look for intelligent, 'natural' immunological approaches? *BMC Immunol.* 18 (2017) 23.
- [2] I.M. Comino-Sanz, M.D. Lopez-Franco, B. Castro, P.L. Pancorbo-Hidalgo, The role of antioxidants on wound healing: a review of the current evidence, *J. Clin. Med.* 10 (2021).
- [3] E.M. Tottoli, R. Dorati, I. Genta, E. Chiesa, S. Pisani, B. Conti, Skin wound healing process and new emerging Technologies for skin wound care and regeneration, *Pharmaceutics* 12 (2020).
- [4] M. Rodrigues, N. Kosaric, C.A. Bonham, G.C. Gurtner, Wound healing: a cellular perspective, *Physiol. Rev.* 99 (2019) 665–706.
- [5] T. Wang, R. Guo, G. Zhou, X. Zhou, Z. Kou, F. Sui, C. Li, L. Tang, Z. Wang, Traditional uses, botany, phytochemistry, pharmacology and toxicology of Panax notoginseng (Burk.) F.H. Chen: a review, *J. Ethnopharmacol.* 188 (2016) 234–258.
- [6] T.B. Ng, Pharmacological activity of sanchi ginseng (Panax notoginseng), *J. Pharm. Pharmacol.* 58 (2006) 1007–1019.
- [7] J. Qu, N. Xu, J. Zhang, X. Geng, R. Zhang, Panax notoginseng saponins and their applications in nervous system disorders: a narrative review, *Ann. Transl. Med.* 8 (2020) 1525.
- [8] D. Wang, L. Lv, Y. Xu, K. Jiang, F. Chen, J. Qian, M. Chen, G. Liu, Y. Xiang, Cardioprotection of Panax Notoginseng saponins against acute myocardial infarction and heart failure through inducing autophagy, *Biomed. Pharmacother.* 136 (2021) 111287.
- [9] S.Y. Men, Q.L. Huo, L. Shi, Y. Yan, C.C. Yang, W. Yu, B.Q. Liu, Panax notoginseng saponins promotes cutaneous wound healing and suppresses scar formation in mice, *J. Cosmet. Dermatol.* 19 (2020) 529–534.
- [10] A.J. Rosenbaum, S. Banerjee, K.M. Rezak, R.L. Uhl, Advances in wound management, *J. Am. Acad. Orthop. Surg.* 26 (2018) 833–843.
- [11] C. Ryall, S. Duarah, S. Chen, H. Yu, J. Wen, Advancements in skin delivery of natural bioactive products for wound management: a brief review of two decades, *Pharmaceutics* 14 (2022).
- [12] D. Jiao, Y. Liu, T. Hou, H. Xu, X. Wang, Q. Shi, Y. Wang, Q. Xing, Q. Liang, Notoginsenoside R1 (NG-R1) promoted lymphatic drainage function to ameliorating rheumatoid arthritis in TNF-tg mice by suppressing NF-kappaB signaling pathway, *Front. Pharmacol.* 12 (2021) 730579.
- [13] G. Lopez-Castejon, D. Brough, Understanding the mechanism of IL-1beta secretion, *Cytokine Growth Factor Rev.* 22 (2011) 189–195.
- [14] M.R. Kandadi, Y. Hua, M. Zhu, S. Turdi, P.W. Nathanielsz, S.P. Ford, S. Nair, J. Ren, Influence of gestational overfeeding on myocardial proinflammatory mediators in fetal sheep heart, *J. Nutr. Biochem.* 24 (2013) 1982–1990.
- [15] R. Wang, M. Lechtenberg, J. Sendker, F. Petereit, A. Deters, A. Hensel, Wound-healing plants from TCM: in vitro investigations on selected TCM plants and their influence on human dermal fibroblasts and keratinocytes, *Fitoterapia* 84 (2013) 308–317.
- [16] S. Khunmanee, S.Y. Chun, Y.S. Ha, J.N. Lee, B.S. Kim, W.W. Gao, I.Y. Kim, D.K. Han, S. You, T.G. Kwon, H. Park, Improvement of IgA nephropathy and kidney regeneration by functionalized hyaluronic acid and gelatin hydrogel, *Tissue Eng Regen Med* 19 (2022) 643–658.
- [17] J.W. Luo, C. Liu, J.H. Wu, L.X. Lin, H.M. Fan, D.H. Zhao, Y.Q. Zhuang, Y.L. Sun, In situ injectable hyaluronic acid/gelatin hydrogel for hemorrhage control, *Mater. Sci. Eng., C* 98 (2019) 628–634.
- [18] L.X. Lin, J.W. Luo, F. Yuan, H.H. Zhang, C.Q. Ye, P. Zhang, Y.L. Sun, In situ cross-linking carbodiimide-modified chitosan hydrogel for postoperative adhesion prevention in a rat model, *Mater. Sci. Eng., C* 81 (2017) 380–385.
- [19] Z. Lu, J. Gao, Q. He, J. Wu, D. Liang, H. Yang, R. Chen, Enhanced antibacterial and wound healing activities of microporous chitosan-Ag/ZnO composite dressing, *Carbohydr. Polym.* 156 (2017) 460–469.
- [20] J. Yang, Z. Chen, D. Pan, H. Li, J. Shen, Umbilical cord-derived mesenchymal stem cell-derived exosomes combined pluronic F127 hydrogel promote chronic diabetic wound healing and complete skin regeneration, *Int. J. Nanomed.* 15 (2020) 5911–5926.
- [21] E. Zudaire, L. Gambardella, C. Kurcz, S. Vermeren, A computational tool for quantitative analysis of vascular networks, *PLoS One* 6 (2011) e27385.
- [22] S. Ning, J. Zang, B. Zhang, X. Feng, F. Qiu, Botanical drugs in traditional Chinese medicine with wound healing properties, *Front. Pharmacol.* 13 (2022) 885484.
- [23] Y. Zhi, H. Wang, B. Huang, G. Yan, L.Z. Yan, W. Zhang, J. Zhang, Panax Notoginseng Saponins suppresses TRPM7 via the PI3K/AKT pathway to inhibit hypertrophic scar formation in vitro, *Burns* 47 (2021) 894–905.
- [24] L. Zhang, Q. Hu, H. Jin, Y. Yang, Y. Yang, R. Yang, Z. Shen, P. Chen, Effects of ginsenoside Rb1 on second-degree burn wound healing and FGF-2/PDGF-BB/PDGF-beta pathway modulation, *Chin. Med.* 16 (2021) 45.
- [25] S.D. Fitzmaurice, R.K. Sivamani, R.R. Isseroff, Antioxidant therapies for wound healing: a clinical guide to currently commercially available products, *Skin Pharmacol. Physiol.* 24 (2011) 113–126.
- [26] K. Raziyeva, Y. Kim, Z. Zharkinbekov, K. Kassymbek, S. Jimi, A. Saparov, Immunology of acute and chronic wound healing, *Biomolecules* 11 (2021).
- [27] F. Zarei, M. Soleimanejad, Role of growth factors and biomaterials in wound healing, *Artif. Cells, Nanomed. Biotechnol.* 46 (2018) 906–911.
- [28] D.B. Gurevich, D.T. David, A. Sundararaman, J. Patel, Endothelial heterogeneity in development and wound healing, *Cells* 10 (2021).
- [29] D. Mehta, R.D. Granstein, Immunoregulatory effects of neuropeptides on endothelial cells: relevance to dermatological disorders, *Dermatology* 235 (2019) 175–186.
- [30] S. Gunes, S. Tamburaci, M.C. Dalay, I. Deliloglu Gurhan, In vitro evaluation of Spirulina platensis extract incorporated skin cream with its wound healing and antioxidant activities, *Pharm. Biol.* 55 (2017) 1824–1832.
- [31] J.S. Low, K.K. Mak, S. Zhang, M.R. Pichika, P. Marappan, K. Mohandas, M.K. Balijepalli, In vitro methods used for discovering plant derived products as wound healing agents - an update on the cell types and rationale, *Fitoterapia* 154 (2021) 105026.
- [32] D. Wang, Q. Jie, B. Liu, Y. Li, L. Dai, J. Luo, L. Hou, Y. Wei, Saponin extract from Panax notoginseng promotes angiogenesis through AMPK- and eNOS-dependent pathways in HUVECs, *Mol. Med. Rep.* 16 (2017) 5211–5218.
- [33] X. Zhou, Y. Guo, K. Yang, P. Liu, J. Wang, The signaling pathways of traditional Chinese medicine in promoting diabetic wound healing, *J. Ethnopharmacol.* 282 (2022) 114662.
- [34] J. Dai, J. Shen, Y. Chai, H. Chen, IL-1beta impaired diabetic wound healing by regulating MMP-2 and MMP-9 through the p38 pathway, *Mediat. Inflamm.* 2021 (2021) 6645766.
- [35] Y. Chang, Y. Wang, J. Liu, X. Chen, X. Ma, Y. Hu, H. Tian, X. Wang, C. Mu, Glucosamine-loaded injectable hydrogel promotes autophagy and inhibits apoptosis after cartilage injury, *Heliyon* 9 (2023) e19879.
- [36] C. Huang, L. Dong, B. Zhao, Y. Lu, S. Huang, Z. Yuan, G. Luo, Y. Xu, W. Qian, Anti-inflammatory hydrogel dressings and skin wound healing, *Clin. Transl. Med.* 12 (2022) e1094.

- [37] Y. Liang, J. He, B. Guo, Functional hydrogels as wound dressing to enhance wound healing, *ACS Nano* 15 (2021) 12687–12722.
- [38] S. Hamed, Y. Ullmann, M. Belokopytov, A. Shoufani, H. Kabha, S. Masri, Z. Feldbrin, L. Kogan, D. Kruchevsky, R. Najjar, P.Y. Liu, J.C. Kerihuel, S. Akita, L. Teot, Topical erythropoietin accelerates wound closure in patients with diabetic foot ulcers: a prospective, multicenter, single-blind, randomized, controlled trial, *Rejuvenation Res.* 24 (2021) 251–261.
- [39] M.A. Nilforoushzadeh, M.M. Sisakht, M.A. Amirkhani, A.M. Seifalian, H.R. Banafshe, J. Verdi, M. Nouradini, Engineered skin graft with stromal vascular fraction cells encapsulated in fibrin-collagen hydrogel: a clinical study for diabetic wound healing, *J. Tissue Eng. Regen. Med.* 14 (2020) 424–440.